

# DIRECT MICROLENSING-REVERBERATION OBSERVATIONS OF THE INTRINSIC MAGNETIC STRUCTURE OF AGN IN DIFFERENT SPECTRAL STATES - A TALE OF TWO QUASARS

Rudolph E. Schild<sup>1</sup>, Darryl J. Leiter<sup>2</sup>, and Stanley L. Robertson<sup>3</sup>

## ABSTRACT

We show how direct microlensing-reverberation analysis performed on two well-known Quasars (Q2237 - The Einstein Cross and Q0957 - The Twin) can be used to observe the inner structure of two quasars which are in significantly different spectral states. These observations allow us to measure the detailed internal structure of quasar Q2237 in a radio quiet high-soft state, and compare it to quasar Q0957 in a radio loud low-hard state. We find that the observed differences in the spectral states of these two quasars can be understood as being due to the location of the inner radii of their accretion disks relative to the co-rotation radii of rotating intrinsically magnetic supermassive compact objects in the centers of these quasars.

*Subject headings:* Galaxies: Quasars: structure: individual: Q2237+0305 — accretion discs: magnetic fields — black hole physics — gravitational lensing: microlensing

## 1. Introduction

An important fundamental issue confronting the study of AGN and Galactic Black Hole Candidates (GBHC) is the fact that these objects are observed to exist in different spectral states. The phenomenon of spectral state switching was first discovered in neutron star X-ray binaries where it was explained in terms of magnetic propeller effects associated with

---

<sup>1</sup>Center for Astrophysics, 60 Garden Street, Cambridge, MA 02138

<sup>2</sup>Marwood Astrophysical Research Center, Charlottesville, VA 22963

<sup>3</sup>Dept. of Physics, Southwestern Oklahoma State University, Weatherford, OK 73096

the interaction of the intrinsic magnetic moment of the of the neutron star with its accretion disk (Ilarianov & Sunyaev, 1975) Spectral state switching was later observed in GBHC where it was found (Robertson and Leiter, 2002, 2003, 2004, 2005) that it could be explained in terms of magnetic propeller effects associated with the interaction of the intrinsic magnetic moment of the GBHC, generated by the central highly red shifted "Magnetospheric Eternally Collapsing Object" (MECO) within it, with the GBHC accretion disk. In these papers it was shown that a unified explanation of spectral properties of GBHC in Radio Loud Low Hard States and Radio Quiet High Soft States can be given as being dynamically generated by the relative location of the inner magnetospheric radii of their accretion disks, with respect to the co-rotation radius associated with the intrinsically magnetic MECO at their centers. A qualitative description of this switching has also been given by Bellon1 (2007).

Recent observations, associated with the effects of intrinsic magnetic propeller interactions generated by MECO in quasars, have been discussed by Schild, Leiter, and Robertson, 2006, hereafter referred to as SLR06, in which intensive gravitational microlensing observations of quasar Q0957 were described which permitted a reconstruction of this quasars inner radiation emitting structures. Surprisingly these observations did not reveal the expected accretion disk extending in close to the central object. Instead the inner accretion disk was observed to be truncated at a very large inner radius. The hot inner edge of the truncated accretion disc appears to be dominated by a very thin plasma annulus, whose thermal radiation is responsible for the "small blue bump" of the quasar spectral energy distribution. In addition, large conical outflow structures were observed about ten times further out from the disk's inner radius.

The overall morphology of these dynamic structures was found to be similar to features revealed in simulated accretion flows onto a compact Young Stellar Object which contains a central rotating magnetic dipole object inside of the accretion disk. Since black holes do not contain observable intrinsic dipole fields, such dynamic structures cannot be generated by black hole-accretion disk models. Hence the conclusion was that we were observing the physical effects of an intrinsic magnetic propeller interaction of a central compact magnetic object in Q0957, and that instead of a black hole the super-massive compact object in this quasar was a MECO. (For a review of the observational and theoretical arguments involved in reaching this conclusion about quasar Q0957 see Appendix I).

Current observations of galactic black hole candidates (GBHC) and active galactic nuclei (AGN) have begun to suggest that the existence of different spectral states, associated with the presence or absence of intrinsic magnetic propeller effects, may play an important role in explaining the broad range in observed AGN properties (radio and hard X-ray emission, UV optical brightness). In this context we will show in this paper how the application of

combined direct microlensing-reverberation analysis on two well known multiple image based quasars (Q2237 - The Einstein Cross and Q0957 -The Twin) can be used to determine the detailed inner structure of two quasars which are in significantly different spectral states.

Sections 1-3 of this paper will show how this combined observational technique allows us to measure the internal structure of quasar Q2237 in a radio quiet high-soft state, and compare it to the internal structure which has been observed in quasar Q0957 in a radio loud low-hard state (SLR06). In sections 4 and 5 we then proceed to analyze the data associated with these observed internal quasar structures of these two quasars in the context of mass scaled versions of recently developed theoretical models (Robertson and Leiter 2002, 2003, 2004, 2005) of Galactic Black Hole Candidates (GBHC) that have the ability to describe spectral state switching between a "Radio Loud Low-Hard State" (low level of soft X-ray emission and strong hard X-ray emission plus strong radio emission) and a "Radio Quiet High-Soft State" (high level of soft X-ray emission but low level of hard X-ray emission, with only a weak level radio emission). In this manner we show how direct microlensing-reverberation analysis allows us to obtain a deeper insight into the fundamental physics which underlies the observational fact that quasars, AGN, and GBHC are observed to be able to occupy a common set of different spectral states. These spectral states, which have properties that scale with the mass of the central compact object, can be classified by observable characteristics such as: strong or weak radio emission, hard or soft X-ray fluxes, and the presence or absence of broad relativistic  $Fe - K(\alpha)$  lines.

For GBHC at low red shift the internal structures responsible for the different spectral states are too small to be resolved at the wavelengths available with current technology. On the other hand for quasars, which are observed at cosmological distances, it has been found that a combination of direct reverberation, microlensing, and nano-lensing techniques are able to resolve the internal quasar structures associated with their spectral states (SLR06).

While individual GBHC objects are observed to switch between the spectral states on time scales of minutes, for AGN and quasars the time scale for the spectral switching process is expected to be the order of years; hence the individually observed AGN will appear to be "frozen" in one state or the other.

Reverberation analysis has proved to be an important technique for the study of Active Galactic Nuclei (AGN) because it can define the characteristics of the complex internal structures in the highly relativistic inner regions which are still too compact to be resolved by direct imaging. The original application by Peterson et al (1991, 1993) showed that a lag between brightness changes of the continuum and emission line regions can be interpreted to indicate the length scale between the regions. Reverberation of the UV-optical continuum light with itself was also discovered, and shown in Q0957 to indicate the existence of internal

structure on time scales of 50 days (Schild & Thomson 1997; S05). In addition, reverberation of the  $2\mu\text{m}$  emission against the continuum in NGC 5548 showed that the near-IR emission comes from a region just beyond the broad line region (Suganuma et al, 2004; see similar result for NGC4151 in Swain et al, 2003; Minezaki et al 2004).

The reverberation analysis in Q0957 seems particularly interesting because it shows the existence of several non-standard forms of internal structures at lags that seem consistent with emission from the Elvis structures that give rise to the broad emission lines (SLR06). The existence of the pattern stream was inferred from auto-correlation analysis applied to the long brightness record accumulated by Schild and colleagues (Schild & Thomson, 1995) for the gravitationally lensed multiple image Q0957+561 A,B quasar. A combination of auto-correlation analysis and reverberation methods was required in the analysis of Q0957 since its pattern of intrinsic brightness fluctuations was quite complex, with several pattern streams overlapping to an extent that prevented single patterns from being easily recognized.

Fortunately the growing brightness record accumulated from photometric monitoring of the Einstein Cross 4-image gravitational lens Q2237+0305 has shown an unambiguous pattern of brightness peaks that confirm the inferences previously made for Q0957, and allows the relative brightness of the peaks to be estimated. This allowed us to clarify the relationship of the peaks to the internal quasar structures, and also provides unique information on the orientation of the quasar in space with respect to the plane of the sky. In the following section, we will show that in the Q2237+0305 quasar lens, an initial outburst in the central region is followed by reverberations interpreted as fluorescent repeats of the central disturbance, since within reasonable limits they have the same amplitude and time scales. From these we will estimate the size, spacing, and orientation of the UV-optically luminous structures in the Q2237 quasar. We will then show that our size estimates are consistent with direct microlensing estimates of quasar size. In particular our reverberation size scale estimates will be shown to be consistent with the Vakulik et al (2007) estimates of the brightness and size scales of the Q2237 inner UV-optical structure.

## 2. Determination of Quasar Intrinsic Brightness Peak Lags

Our approach to the determination of the Q2237 structure parameters follows closely the procedure outlined for the Q0957 quasar (S05; SLR06). The procedure is a variant of the reverberation analysis first applied by Peterson et al (1991,1993) to NGC 5548; however their observations and analysis were of the reverberation between the optical continuum and the emission lines. In our implementation for Q0957, reverberation of the continuum emission by itself was discovered by Schild and Thomson (1997), wherein it was

noticed that multiple peaks are found in the autocorrelation estimates of the long Q0957 brightness record compiled by Schild and Thomson (1995). The actual succession of peaks evidencing the reverberations have not been identified in the Schild et al brightness data records, because of irregular data sampling, and because many overlapping patterns are seen throughout the Q0957 brightness record. However in Q2237, where 4 quasar images and the central galaxy are clearly seen in the well-known Einstein Cross pattern, identical brightness peaks are clearly evident, and these have been exploited by Vakulik et al (2006) to determine the very short (approximately 1 day) time delay lags of the overall strong gravitational lensing configuration. The excellent photometric data and their plot can be seen at (<http://www.astrouw.edu.pl/~ogle/ogle3/huchra.html>) (Wozniak et al. (2000)). In their colored plot of the image brightness, the first brightening pulse must have occurred at approximately  $\text{HJD}-2450000 = 2550$ , although the actual mid-point and profile of the initial event are obscured because of poor sampling at the time. The event is signaled by a brightness increase of 0.3 magnitudes for a duration of approximately 150 days. This was especially well seen in the data for image A (green data points). The A image is apparently undergoing a sustained period of low amplitude microlensing whose peak was previously seen in the OGLE I data set (<http://bulge.princeton.edu/~ogle/ogle2/huchra.html>)(Wozniak et al 2000). Although the peak is defined by brightness measured near the beginning and end only in the OGLE III data set, additional data from Koptelova et al (2004) show that the brightness was constant during that observing season for all four quasar images.

The new quasar intrinsic brightening event can probably also be recognized in the B, C, and D images, which causes us to conclude that it is an intrinsic quasar brightening event, not a microlensing artifact. The first peak was followed 415 days later by another peak of comparable brightness at 2965 days, again particularly well seen in the A image green brightness record. This nearly simultaneous rise in all four images was the observational basis for the determination of the time delays of the four images by Vakulik et al, 2006. These authors analyzed the V-band OGLE III data but also their own R-band data, which had somewhat lower brightness peak amplitudes. The lags determined were approximately one day, as expected. The brightness amplitude, about 0.3 magnitudes, and event duration, approximately 100 days, were all comparable to, but slightly lower than, the initial peak. A third peak can barely be recognized at approximately  $\text{HJD} - 2450000 = 3300$ , but at only half the amplitude of the first two peaks. Nevertheless the duration of the event is the same as for the first two peaks, although the third peak cannot be recognized at all in image B because a microlensing event has evidently distorted the brightness curve. A fourth and somewhat brighter peak can probably be recognized at  $\text{HJD} - 2450000 = 3700$  days, but microlensing of both the A and B images combine with poor sampling because of seasonal observing effects, to observe this feature. In Q2237, a fifth and final pulse might be

recognizable, but it appears to be too weak to distinguish it from the noise associated with microlensing confusion and seasonal data effects. It is evidently weak, as was also inferred for the final autocorrelation peak at 620 days in Q0957 (S05).

We do not consider that the case for the existence of the 2 last peaks is compelling, and we agree that the poor sampling of the light curve at the time of the first peak adds significant uncertainty to the calculation of inclination effects, which will be discussed later in this section. Nevertheless, the fact that these data sets produce a reasonable calculation of the Q2237 strong lensing time lags (Vakulik et al, 2005) inspires confidence that important intrinsic quasar brightening effects have been observed, and even if the quasar fully cooperates, it will be at least 5 years before a comparable event can be fully observed. For this reason application of the calculational procedure, previously used for Q0957 (S05) to these data and the interpretation for the Einstein Cross, Q2237, is fully justified. The observed data appears to present evidence for the existence of a complex interior quasar structure associated with complex physical structures seen in reverberation and having time scales of 3 years as measured by the observer’s clock. Correcting this time scale by  $(1+z) = 2.69$  and converting to size scale at light propagation speed gives reverberation quasar structure scale of approximately 1 light year or  $10^{18}cm$ . In the following paragraphs we will show that a full analysis of this data, including allowance for inclination effects, gives a measurement of the distance from the central object to the Elvis structure whose value is determined to be  $8.4 \times 10^{17}cm$ .

We demonstrate next that if we adopt the series of brightness peaks as continuum reverberations from the various internal quasar structures as was done previously for Q0957 (S05 and SLR06), we can calculate a self-consistent quasar picture that determines the locations and sizes of the quasar structures, and also determines the inclination of the quasar to the line of sight. To do this we adopt the series of 4 equations from S05 for three unknown parameters which imply an over-constrained problem. However because of the large uncertainties in the adopted lags, we do not propose an elaborate statistical analysis for the uncertainty of the derived parameters. The adopted physical quasar model includes an Elvis (2000) outflow structure which is luminous in the UV-optical continuum, and which effectively produces a luminous ring above the accretion disc plane, and a second ring below. The geometry of this structure is shown graphically in the two Q0957 references cited above and in Fig 1 of this paper. In the context of this analysis the outer structure produces most of the quasar’s UV-optical luminosity. Referring back to the quasar brightness history published by the OGLE III research group, we see that the event marking time zero, which is probably an energy deposition in the quasar’s corona- like central region or perhaps at the inner edge of the accretion disc, produces a 30% brightness increase. This is followed by reverberation off the 4 surfaces of 25%, 10%, 10%, and 5%, so in a sense 80% of the quasar’s

UV-optical luminosity is apparently contributed by these quasar structures. These numbers for the brightness peaks in the first and subsequent reverberations are nicely confirmed by the Vakulik et al (2007) simulation of the observed microlensing events seen in the OGLE III brightness curves. Because the nearby location of the microlensing galaxy makes the microlensing sensitive to the smaller interior structure and hardly sensitive to large outer structure on time scales of available data, and because the amplitudes of the cusp-shaped microlensing events must be caused by stars and can only represent a fraction of the quasar luminosity, the Vakulik et al (2007) results give a direct measure of the fraction of the quasar luminosity contributed by the central structure, which, taking the orientation angle between the observer’s line of sight and the quasar’s polar axis angle into account, has a radial size estimated from the simulation as  $1.9 \times 10^{15} \text{ cm}$ .

These Vakulik et al (2007) simulations show that this compact inner structure contributes only half as much UV-optical continuum radiation, as measured with the V filter of the OGLE-III monitoring program, as the large outer structure. In other words, the inner structure contributes only 1/3 of the total quasar luminosity. In the preceding paragraph, we estimated that the first impulse observed in the brightness stream was only about 30% of the total quasar brightness. The estimates are thus consistent. Notice that the two estimates are independent, one directly from the observed brightness record, while the other one is from a statistical microlensing simulation.

For brevity we do not here repeat the equations solved for the quasar structure and inclination; they are given, together with an illustration showing their definition, in Schild (2005, Fig. 1). Solutions to this set of equations were expressed in triads of  $(r, \theta, \epsilon)$ . Here  $r$  is the quasar structure variable giving the radial distance between the compact central object and the luminous surface of the Elvis structure. Variable  $\theta$  is the quasar orientation variable, expressed as the angular distance between the observer’s line of sight and the quasar’s polar axis. Angle  $\epsilon$  is the internal structure variable expressing the angle between the radius to the luminous Elvis surface and the accretion disc plane.

As described in S05, two possible solutions occur because of the unique geometry associated with the centrally illuminated Elvis structure. In both cases, the first arriving reverberation is from the region of the Elvis structure closest to the observer. Then case 2 is when the second reverberation is from the part of the Elvis structure farthest from the observer but on the same side of the accretion disc, whereas case 1 is when the second reverberation is from the nearest portion on the opposite side of the accretion disc. It will always be true that case 1 is statistically more probable than case 2, since there is just a low probability that the quasar pole is nearly aligned with the observers line of sight to the quasar. This is of course true only to the extent that the quasars have not been selected by

some orientation-dependent criterion, like the beaming of the radio jet.

Our case 1 solution with  $(r, \theta, \epsilon)$  of  $(8.4 \times 10^{17} \text{ cm}, 21 \text{ deg}, 10.7 \text{ deg})$  has its luminous Elvis structure rings  $1.6 \times 10^{17} \text{ cm}$  above the accretion disc plane. The case 2 solution with  $(8.4 \times 10^{17} \text{ cm}, 10.7 \text{ deg}, 21 \text{ deg})$  features the Elvis structure ring  $3.0 \times 10^{17} \text{ cm}$  above (and below) the accretion disc plane. For both case 1 and case 2, the angle between the observer and the pole of the accretion disc plane is small, although the quasar was optically selected.

In time, better observations of the quasar brightness and color fluctuations will allow discrimination between case 1 and case 2. In both cases, the strongest (brightest) reverberation will always be from the first arriving pulse, because this near-side emitting surface has no absorption and has relativistic beaming of the observed reverberation. The second arriving reverberation in case 2 should be approximately as strong as the first, since it will be seen at a small angle  $\theta$  giving approximately the same relativistic beaming and no absorption. In case 1, the second reverberation is off of the surface beamed away from the observer, and is seen through substantial obscuration. These assertions presume that the dark clouds of the putative dusty torus are contained just beyond the Elvis outflow structures (see Fig. 1), which presumably shield them from the hard emissions of the inner chromosphere and the inner edge of the accretion disc. Recall that reverberation between the  $2.2 \mu\text{m}$  emission and the UV/optical emission reported by Minezaki et al (2003) locate the near-IR emission just outside the Elvis structured continuum emitting region.

From simple inspection of the brightness records for the Q2237 quasar, we see that the second observed reverberation is less than half the amplitude of the first. This tends to favor the case 1 geometry, which we will therefore adopt for the remainder of this report. For case 1 geometry in Q2237, the luminous surfaces of the Elvis structure are determined from our solution to be  $8.4 \times 10^{17} \text{ cm}$  from the compact central source; for the purpose of the modeling calculations to be discussed later in the paper it is important to know how far this is in the accretion disc plane. Multiplying by  $\cos 10.7 \text{ deg}$ , we find that the luminous surfaces lie  $8.2 \times 10^{17} \text{ cm}$  from the center and  $1.6 \times 10^{17} \text{ cm}$  above and below the plane. The opening angle (the angle between the observer’s line of sight and the jet outflow, with the central compact source at the vertex) is 79.3 degrees.

Finally we note that for the solution of the structure equations proposed above, we can predict the arrival time of the final brightness peak. In either case 1 or case 2 orientation, the final peak should arrive 1332 days (observer’s clock) following the initial outburst.



### 3. Image Brightness Enhancement Corrections to the Observed Fluxes From Q2237 and Q0957

Because the multiple images associated with gravitational lenses are usually separated by only a few arc seconds in the plane of the sky, historically observations of them at some wavelengths require correction for the number of images if the intrinsic quasar luminosity is to be inferred from a brightness measurement of the combined image. Furthermore, the lensed images are magnified by the lensing, so determination of the intrinsic quasar fluxes requires a correction for the magnification. Accurate knowledge of the fluxes is important to our analytical model of the quasar structure as summarized in Tables 1 and 2. Then as discussed in section 4 below, if the distantly observed MECO period of rotation can be estimated from observations of the outer light cylinder radius of the MECO, the analytical model then allows us to estimate the MECO mass, accretion rate, and magnetic field strength (with rotation rate estimated from the light cylinder radius)

#### 3.1. Image Brightness Corrections to the Observed Flux of Q2237

For Q2237 in the radio quiet high soft state, four images are seen and so the published total radio flux estimate for the entire system must be divided by four. While the magnification factor is still uncertain, the most recent models by Schmidt and Wambsganss (2004) suggest a magnification factor of sixteen. Early radio observations of the Einstein Cross concluded that the quasar was radio quiet, but a more heroic 11 hour integration with the VLA in A configuration produced a 3.6 cm total flux measurement of  $593 \pm 88$  micro-Janskys (Falco et al 1998). With correction of factor 4 for the image multiplicity and 16 for strong lensing magnification, the inferred quasar 3.6 cm radio flux is 9.3 micro-Janskys, which puts it in the class of radio quiet quasars.

The X-ray luminosity of Q2237 has been measured in two Chandra observations over the 0.4 - 8.0 Kev band reported by Dai et al (2004). Their uncorrected total flux measurement of  $9.2 \times 10^{45}$  ergs/sec must be corrected by 4 for the image multiplicity and by factor 16 for strong lensing; we adopt a corrected quasar X-ray luminosity of  $1.4 \times 10^{44}$  erg/sec. An important discovery of the Chandra observation of Q2237 was the observation of a red shifted broad  $FeK_{\alpha}$  line at 5.7 KeV. The estimated FWHM is 0.87 KeV and equivalent width is 1200 eV. Thus for a rest wavelength of 8.7 KeV the red shift is 0.52 (velocity  $1.6 \times 10^{10}$  cm/sec) and the velocity width is  $0.45 \times 10^{10}$  cm/sec (45,000 km/sec). Because the line is prominent in image A and unseen or weak in images B, C, and D, it must be microlensed, as discussed by Popovic et al(2006), who conclude that the region emitting the emission line must be smaller than the continuum emitting region, consistent with the suggestion that the line emission

comes from the thin inner edge of the accretion disc. Popovic et al also noticed that because of the short duration and strength of the microlensing event, micro lenses with mass on the order of a planetary mass are required if the central compact quasar mass is on the order of  $3 \times 10^9 M_{\odot}$ , as estimated here.

### 3.2. Image Brightness Corrections to the Observed Flux of Q0957

For Q0957 in a radio loud low hard state, two images are seen and the total flux estimate for the entire system must be divided by two. While the magnification factor is still uncertain the most recent models by Schild & Vakulik (2003), which include the microlensing magnification, suggest an overall brightness amplification factor of three.

Radio observations of the Q0957 have shown that the quasar is radio loud and has a jet whose radio brightness is dominated by the core of the jet. Using a correction of factor 2 for the image multiplicity and a factor 3 for strong lensing magnification. The inferred quasar 6 cm radio flux has been determined to be 9.3 milli-Janskys (Lehar et al 1991, Schild (2005) and Schild, Leiter, and Robertson (2006)) giving Q0957 a radio luminosity of  $3.7 \times 10^{42}$  erg/sec.

The X-ray luminosity of Q0957 has been measured in Chandra observations over the 0.4 - 8.0 Kev band reported by Chartas et al (2001). Their uncorrected total flux measurement of  $1.5 \times 10^{46}$  ergs/sec must be corrected by 2 for the image multiplicity and by factor 3 for strong lensing; we adopt a corrected quasar luminosity of  $2.5 \times 10^{45}$  erg/sec. We also note that an important conclusion of the Chandra observation of Q0957 was the apparent lack of any red shifted broad Fe-Kalpha line at 5.7 KeV.

## 4. Analysis of the Internal Structure of Q2237 and Q0957 in Different Spectral States

In the following sections we will compare the observed inner structure for Q2237 (the Einstein Cross quasar in the radio quiet high soft spectral state) to the inner structure of Q0957 (the Twin quasar in the radio loud low hard spectral state) which was previously established in the 2006 paper by Schild, Leiter, and Robertson. In the process we will find that the explanation of the physical difference between the two quasars Q0957 and Q2237 is related to the more general question as to why some quasars are observed to be radio loud and have a hard X-ray spectrum while others are observed to be radio quiet and have a soft X-ray spectrum. In this section we will compare and analyze the data for these two quasars, as shown in Tables 1 and 2 below, in terms of a new theoretical quasar model which is easily

able to explain the physical nature of these quasars in their different spectral states as well as providing new understanding that can bring unification to a wide body of quasar data.

#### 4.1. Analysis of the Internal Structure of Quasar Q0957 in the Radio Loud Low Hard State (RL-LHS)

We begin by recalling that in SLR06, we examined the empirical data for the lensed and micro-lensed Q0957+561A,B quasar obtained from 20 years of brightness monitoring at visible wavelengths (near-ultraviolet emission at the quasar). In that report we examined several conclusions inferred previously from analysis of the auto-correlation and micro-lensing properties of the monitoring data, and collected these results in a consistent presentation and used them to confront physical quasar models and their simulations. On the basis of the analysis in SLR06 the inner structure observed for the quasar Q0957 in the (RL-LHS), which we referred to as the Schild-Vakulik Structure, was made up of four component parts which had the following dimensional properties (see figure 1):

- 1. Elliptical Elvis Structure:  $R_e = 2 \times 10^{17}\text{cm}$ ,  $H_e = 5 \times 10^{16}\text{cm}$
- 2. Inner Radius of Accretion Disk:  $R_{disk} = 4 \times 10^{16}\text{cm}$
- 3. Hot Inner Accretion Disk Annulus:  $\Delta(R) = 5.4 \times 10^{14}\text{cm}$
- 4. Base of Radio Jet:  $R_{rad} = 2 \times 10^{16}\text{cm}$  ,  $H_{rad} = 9 \times 10^{16}\text{cm}$

The inner components of this quasar structure were found to be an accretion disc truncated at a large radius whose hot inner edge contained a bright thin annulus. This inner structure was found to be surrounded by an elliptical coronal outflow (Elvis Structure) long known to explain the complex spectroscopic behavior observed in quasars. However it was observed that the opening angle of the coronal Elvis structure with respect to the z-axis of rotation appeared to have a very large value of 76 degrees. In addition a radio emission region was found to be located directly above the compact source. The size and location of this radio emitting region was found to be where the reconnection of magnetic field lines at relativistic Alfvén speeds, like that generated by a rotating central object containing an intrinsic magnetic field, should occur. Hence the structure observed in the quasar Q0957+561 appeared to closely resemble the complex inflow-outflow patterns seen in intrinsic magnetic propeller models for young stellar objects (Romanova et al, 2002, 2003a, 2003b, 2004).

In SLR06 it was shown how standard black hole models were unable to account for the internal structure observed in the quasar Q0957. In particular we discussed how attempts

to model the observed internal structure seen in the quasar Q0957+561 in terms of the intrinsic magnetic moment generated by a central spinning charged black hole failed because the necessary charge on the spinning black hole required to make it work would not be stable enough to account for the long lifetime of the observed Schild-Vakulik structure. Similarly it was shown how attempts to model the internal Q0957 structure in terms of Kerr Black Hole-ADAF-Accretion Disc Corona-Jet Models, in which the magnetic field is tied to the accretion disk and not the central rotating compact object, failed in that this model was unable to account for the very large opening angles observed for the coronal Elvis outflows. Finally it was shown that Magnetically Arrested Disc (MAD) black hole models failed in that they predicted the existence of orbiting infalling hot blobs of plasma inside of the inner region of the accretion disk that were not observed.

On the other hand it was shown in SLR06 that the four components of the intrinsically magnetic structure observed in Q0957 could be successfully explained by Magnetospheric Eternally Collapsing Object (MECO) models (Robertson and Leiter 2003, 2004, 2005), which feature highly redshifted, Eddington limited, collapsing central compact objects containing a strong intrinsic magnetic moment aligned with the MECO axis of rotation (see Appendix 1 for more details). This is indicated in Table 1 and Table 2 where, taking into account the amplification factor of three discussed in section 3.b it is shown that the MECO model for the quasar Q0957+561 can be represented by a  $4.2 \times 10^9 M_{\odot}$  mass scaled up version of the class of MECO models that have been used to explain "spectral state switching" phenomena associated with Galactic Black Hole Candidates. Such a massive MECO object does not collapse beyond its event horizon. Instead, in-falling matter heats up and because of its intense radiation collects at a highly redshifted physical surface which is balanced in a state of local Eddington limited secular equilibrium at a radial distance which is just outside of its event horizon. This allows the highly redshifted MECO surface to slowly collapse, while remaining in causal connection outside of its event horizon, over time intervals greater than a Hubble time as seen by a distant observer. Because of the small light cone opening angle for radiation escaping from this highly red shifted MECO surface to a distant observer, the resultant low luminosity in the far-infrared wavelengths make this MECO surface difficult to detect for the case of Q0957+561.

In SLR06 it was demonstrated that Q0957 could be successfully modeled only as a MECO driven quasar in the Low Hard State in which the MECO intrinsic magnetic propeller interacted strongly with the inner regions of the quasar's accretion disc. For Q0957 in the Low Hard State, the dynamo action of the intrinsic rotating MECO magnetic dipole field of its central supermassive MECO sweeps clean the central region of the quasar out to the magnetospheric radius where the magnetic propeller acting on the inner edge of the accretion disc creates a very thin annular band, and a radio emitting region above the

disc where the magnetic field lines twist and bunch up until they eventually break and reconnect at relativistic speeds. The resultant size and location of the radio emitting region associated with this inner magnetic structure of the quasar was found to be in the region above the central supermassive MECO object where the reconnection of magnetic field lines at relativistic Alfvén speeds, like that generated by a rotating central MECO containing an intrinsic magnetic field, should occur.

For the quasar Q0957 the outer bi-conic Elliptical Elvis Coronal Outflow Structure, that was observed to occur with a very wide opening angle above and below the accretion disk at a distance  $R_{Elvis} \sim 2 \times 10^{17}$  cm, was found to be located just inside of the outer light cylinder of its central MECO which occurred at a radial distance of  $R_{lc} \sim 2.4 \times 10^{17}$  cm. See Table 1-2 where this observation, and the formula for the MECO outer light cylinder given by  $R_{lc} \sim (1.5 \times 10^{17} \text{ cm}) \times T_{year}$ , was used to estimate the distantly observed rotation period of the central MECO in Q0957 as  $T_{Year} \sim 1.6$  years.

The existence and the radial location of bi-conic Elliptical Elvis Coronal Outflow Structures, occurring just inside of the outer light cylinders of central compact MECO magnetic objects surrounded by hot accretion disks, is a predicted observational property of the MECO-quasar accretion disk model that uniquely distinguishes it from a black hole-quasar accretion disk model.

The MECO-quasar model satisfies the physical conditions required to generate bi-conic shaped Elvis Outflow Structures just inside of their outer light cylinders by virtue of the combined action of two well-known physical processes: a) Magnetic reconnection effects which can generate upward flows just inside of the outer light cylinder of central compact magnetic objects surrounded by accretion disks (Uzdensky, 2003, 2006; Uzdensky; Spitovsky, 2006), and b) Optical line driving forces, associated with the presence of strong ultraviolet luminosity emitted from the inner magnetospheric radius of a hot accretion disk surrounding the central compact magnetic object, which can act on the magnetic reconnection generated upward flows just inside of the outer light cylinder and there create the bi-conic Elvis Outflow Structures (Elvis 2000, 2003, 2006).

In this manner the intrinsic magnetic field of the MECO generates a vertical up-flow of plasma above the accretion disk by magnetic reconnection effects which occur just inside of the outer light cylinder of the MECO. The vertical up-flow of plasma occurs where the surrounding dusty torus ends and the bi-conic Elvis Outflow Structure begins (see Fig. 1). If the inner accretion disk is hot enough to make UV radiation then the effect of photoionization line-driving bends the upward flowing plasma outward over the accretion disk and generates the bi-conic Elvis Outflow Structure of positive ions associated with the Broad Emission Line Region (BELR). Charge separation between the electrons and outflowing ions

is generated by the photo-ionization process near the MECO light cylinder. The return current of ions most likely flows back to the central region along the separatrix associated with field-line opening due to the differential rotation which occurs in the magnetically-linked MECO disk system.

#### 4.2. Analysis of the Internal Structure of Quasar Q2237 in the Radio Quiet High Soft State

As discussed in sections 3.a the detailed internal structure of quasar Q2237 in a radio quiet high-soft state has been observed to be as follows:

- 1. Elliptical Elvis Structure:  $R_e = 8.2 \times 10^{17} \text{cm}$  ,  $H_e = 5 \times 10^{16} \text{cm}$
- 2. Inner Radius of Accretion Disk:  $R_{disk} = 1.9 \times 10^{15} \text{cm}$
- 3. Broad Iron Line Emission seen: Yes
- 4. Base of Radio Jet: None since there is no jet in Radio Quiet State

In the context of the MECO model the internal structure of the quasar Q2237 can be easily understood in terms of different spectral states (i.e. Radio Loud Low Hard States versus Radio Quiet High Soft States) which are distinguished by the nature of the interaction between the accretion disks in these quasars and the intrinsic rotating magnetic moments of their central supermassive MECO. We begin by recalling that in section 4a we found that for Radio Loud Low Hard States like that seen in Q0957, the magnetospheric radius  $R_m$  is greater than its MECO co-rotation radius  $R_{cr}$  and the resultant magnetic propeller effect on the accretion disk generates an empty inner region inside of the accretion disk, which is surrounded by a thin hot ring, and a jet outflow leading to strong radio emission. However for Radio Quiet High Soft States (RQ-HSS) like that observed in Q2237, the accretion rate is high enough to push the magnetospheric radius  $R_m$  inside of its MECO co-rotation radius  $R_{cr}$ . This shuts down the magnetic propeller, and the jet outflow which creates a spectral change from a RL-LHS to a RQ-HSS state. In this state the intrinsic magnetic propeller mechanism of the MECO-AGN becomes incapable of ejecting the flow in the form of a jet, which causes an increasingly dense boundary layer of plasma to form at the inner disk radius which eventually pushes it in all the way to the marginally stable orbit. When this occurs the MECO-AGN changes its spectral state from a Radio Loud Low Hard State (RL-LHS) to a Radio Quiet High Soft State (RQ-HSS).

To get a better physical insight into the nature of this process let us discuss the dynamics of the MECO-quasar spectral state change from RL-LHS state to the RQ-HSS state in a little more detail. For the higher accretion rates associated with the RQ-HSS the intrinsically rotating MECO magnetic field is dynamically unable to eject the disk material from the interior region inside of the co-rotation radius  $R_{cr}$ , and the accreted matter piles up against the magnetopause and pushes it inward. The fact that a boundary layer at the inner accretion disk radius must exist around a MECO in the (RQ-HSS) was demonstrated (Robertson and Leiter 2005 section 11, pp 24-25) by comparing the magnetic pressure at the magnetosphere with the impact pressure of a trailing, subsonic disk where it was shown that radial inflow disk velocities in excess of the speed of light would be required to allow the impact pressure to match the magnetic pressure. While the gas pressure in the disk at the inner radius of the transition zone is normally required to match the magnetic pressure in the disk, it turns out that for the (RQ-HSS) state the radiation pressure in the disk is less than the gas pressure. Hence for a MECO-AGN in the RQ-HSS the boundary layer, located at the inner disk radius of its gas pressure dominated, thin, subsonic Keplerian disk, will eventually be pushed down to the marginally stable orbit of its accretion disk so that  $R_{disk} \sim R_{ms}$ . The value of  $R_{ms}$  will depend on the  $a/M$  ratio of the rotating Vaidya metric which describes the MECO (which, because of the very highly redshift of the MECO, will to a good approximation be similar to the value of  $R_{ms}$  for a Kerr metric). In order to apply the above analysis to the case of Q2237 in the RQ-HSS we recall from section 3.a that Vakulik et al (2007) found that the fraction of the quasar luminosity contributed by the central structure was associated with a radial size of  $1.9 \times 10^{15} \text{cm}$ . Assuming that this is the inner radius of the luminous accretion disc edge for the case of Q2237 in the RQ-HSS, we find that  $R_{disc} \sim R_m \sim 1.9 \times 10^{15} \text{cm} = 4.2 R_{grav}$ . This is consistent with the central MECO in Q2237 having a mass of  $3 \times 10^9 M_{\odot}$  and a specific angular momentum ratio of  $a/M = 0.5$ . In this context we find that the observed core X-ray luminosity of  $L_x \sim 1.4 \times 10^{44} \text{erg/sec}$ , which in the RQ-HSS is generated in the corona above the accretion disk, will interact with the inner region of the accretion disk and generate broad Iron emission lines consistent with Q2237 observation.

In addition we find that the properties of MECO-quasar model for Q2237 satisfy the physical conditions required to generate bi-conic shaped Elvis Outflow Structures just inside of their outer light cylinders by virtue of the combined action of magnetic reconnection effects (which generate upward flows just inside of the light cylinder of central compact magnetic objects surrounded by accretion disks) and optical line driving forces (associated with the presence of strong ultraviolet luminosity emitted from the inner magnetospheric radius of a hot accretion disk surrounding the central compact magnetic object) which act on the magnetic reconnection generated upward flows that occur just inside of the outer light cylinder and there create the bi-conic Elvis Outflow Structure observed. For the case of the

quasar Q2237 the outer bi-conic Elvis Outflow Structure, with a very wide opening angle, which was observed above and below the accretion disk at a distance  $R_{Elvis} \sim 8.2 \times 10^{17} \text{cm}$ , is found to be located just inside the outer light cylinder of its central MECO at  $R_{lc} \sim 8.4 \times 10^{17} \text{cm}$  (note that this result is obtained from  $R_{lc} \sim (1.5 \times 10^{17} \text{cm}) \times T_{year}$ , where  $T_{year}$  is the distantly observed rotation period of the central MECO, which for the case of Q2237 was found to be  $T_{year} \sim 5.6$  years). It is important to note that the existence of bi-conic Elliptical Elvis Coronal Outflow Structures, predicted to occur just inside of the outer light cylinders of central compact MECO magnetic objects surrounded by hot accretion disks, is a key observational prediction of the MECO-quasar accretion disk models which distinguishes it from black hole-quasar accretion disk models.

## 5. CONCLUSIONS

We have shown how direct microlensing-reverberation analysis performed on two well-known Quasars (Q2237 - The Einstein Cross and Q0957 - The Twin) can be used to determine the inner structure of two quasars which are in significantly different spectral states. These observations allowed us to measure the detailed internal structure of quasar Q2237 in a radio quiet high-soft state, and compare it to quasar Q0957 in a radio loud low-hard state. We found that a unified explanation of the dynamics of the inner and outer components of the observed internal structure of these two quasars could be dynamically explained as being due to different spectral states (i.e. Q0957 in a Radio Loud Low Hard State (RL-LHS), and Q2237 in a Radio Quiet High Soft State (RQ-HSS)). We then argued that when taken together, the most plausible physical explanation for the observed differences in the spectral states of these two quasars was due to the location of the inner radii of their accretion disks (see Fig. 2) relative to the co-rotation radii associated with supermassive, rotating "Magnetospheric Eternally Collapsing Objects" (MECO) in the centers of these quasars (ref Appendix I).

In support of the above argument we first described the unique gravitational microlensing observations of the quasar Q0957 in the (RL-LHS) which permitted a reconstruction of its internal radiation emitting structures (SLR06). In the context of these observations the inner accretion disk was found to be truncated at a very large radius and surrounded by a very thin hot inner ring of plasma with a large empty inner region inside of it. In addition large bi-conic Elvis outflow structures were observed about ten times further out from the inner disk radius. The overall morphology of these dynamic structures were found to be similar to features revealed in simulated accretion flows into compact Young Stellar Objects which contain a central rotating magnetic dipole objects inside of their accretion



disks (Romanova 2002, 2003a). Since black holes do not contain observable intrinsic dipole fields, such dynamic structures cannot be generated by black hole-accretion disk models. Hence our conclusion was that we were observing the physical effects of a central supermassive compact intrinsically magnetic object in Q0957, and that instead of a black hole the super-massive compact object in this quasar was a MECO

Then applying the MECO model to the case of Q2237 in the (RQ-HSS), we argued that the higher accretion rates involved pushed the inner magnetospheric radius of its accretion disk through the co-rotation radius of its central MECO and shut down the MECO magnetic propeller effect on the accretion disk. Since the lack of magnetic propeller action on the accretion disk turned off the radio-jet emission leading to the creation of a radio quiet state, and caused the inner radius of the accretion disk to be pushed down to the marginally stable orbit, then X-rays generated in the corona above the accretion disk were able to act on the inner edge of the accretion disk and create the broad iron line 9.7 Kev signature observed in Q2237. In support of this idea we note that models of the inner region surrounding the inner accretion disc edge, for young stellar objects by Romanova (2002, 2003a,b; 2004) and others, feature an inner corona of ionized matter above the accretion disk.

Detailed calculations from analytical modeling shown in Table 1-2, showed how the MECO model can quantitatively explain the inner dynamic structures of both the quasar Q0957 in a RL-LHS state as well as that of the quasar Q2237 in a RQ-HSS state. In the MECO model the different spectral states of these two quasars were determined by the magnitude of their respective accretion rates and the interaction between their accretion disks and the intrinsic rotating magnetic moments of their central supermassive MECO. In addition the MECO model for Q0957 and Q2237 connected the location of their Elvis outflow structures to the location of the outer light cylinders of their central rotating supermassive MECO.

The MECO model of internal quasar structure presented here, for Q0957 in the radio loud low hard state and Q2237 in the radio quiet high soft state, can be readily applied to a wide body of data on other quasars observed in one or the other of these two spectral states and for this reason has the potential to be able to unify a vast amount of quasar spectroscopic and photometric data.

In addition the MECO quasar model has the unique property of dynamically connecting the location of the inner part of the quasar Elvis outflow structure with the location of the outer light cylinders of the central MECO in these quasars. Because of the special geometric relationship that elliptical Elvis outflow structures have to the modified dusty torus components of their Elvis structures as shown in figure 1, the MECO quasar model predicts that for any orientation of the quasar to the line of sight, some component of emission

should be evident for any optical depth of dusty torus absorption. This result is based on the assumption that the continuum emission originates principally in a corona near the inner edge of the accretion disc, and at the outflow structures illuminated by the inner corona and accretion disc. This is because in MECO quasar model, the Elvis structures form the inner edge of the dusty torus. Then for all viewing angles the UV-optical power-law continuum should be visible, except possibly for extreme equator-on geometry (with the pole of the accretion disc perpendicular to the line of sight.)

In summary we have demonstrated how direct microlensing-reverberation analysis of two Quasars (Q2237 - The Einstein Cross and Q0957 - The Twin) have allowed us to observe inner structure of two quasars which are in significantly different spectral states. Standard black hole accretion disk models were found to be unable to offer a unified dynamical explanation of the observed internal structure of both of these two quasars in different spectral states. Instead we found that a unified explanation could be obtained within the framework of a MECO model. This was done by describing the spectral states of the two quasars in terms of the location of the magnetospheric radii of their accretion disks with respect to the co-rotation radii, inside of the light cylinder surrounding highly red shifted, rotating  $M \sim 10^9 M_{\odot}$  MECO in the centers of these quasars.

Because of the apparent ease with which the size of the Elvis structure and the quasar orientation with respect to the plane of the sky can be inferred, following the method of S05, future photometric observations with the planned Large Scale Synoptic Telescope (LSST) will allow an important MECO parameter to be easily obtained for any of the thousands of quasars to be monitored. Since the radius of the MECO outer light cylinder depends only on the distantly observed MECO period of rotation, the connection between the MECO outer light cylinder and the location of the Elvis outflow structures observationally determines the distantly observed MECO spin parameter. Hence, in addition to the MECO mass and intrinsic magnetic moment, simple recognition of patterns of reverberations and their timing allows distantly observed MECO spin parameters to be obtained.

## 6. APPENDIX I. THE STRONG PRINCIPLE OF EQUIVALENCE AND MAGNETOSPHERIC ETERNALLY COLLAPSING OBJECTS (MECO)

In General Relativity, preservation of the Strong Principle of Equivalence (SPOE) requires that Special Relativity must hold locally for all time-like observers in all of space-time. The existence of MECO is implied by the idea that Nature requires that the Strong Principle of Equivalence (SPOE) be dynamically preserved everywhere in space-time for the timelike world lines of massive particles or fluids under the influence of both gravitational and non-

gravitational forces. Preservation of the SPOE requires that the frame of reference of the co-moving observer in the massive collapsing fluid must always be connected to the frame of reference of a stationary observer by special relativistic transformations with a physical 3-speed that is less than the speed of light (SLR06 and Landau & Lifshitz, 1975). Since the left hand side of the Einstein equation cannot by itself enforce the dynamic preservation of the SPOE then SPOE-preserving non-gravitational processes must exist in Nature and must always be included in the energy-momentum tensor on the right hand side of the Einstein equation.

It was in this context that the general relativistic MECO solutions to the Einstein-Maxwell equations were discovered, as was shown in the three previously published papers of Robertson and Leiter and developed in more detail in Appendix 1-10 of astro-ph/0505518. There it was shown that for a collapsing body, the structure and radiation transfer properties of the energy-momentum tensor on the right hand side of the Einstein field equations, could describe a collapsing radiating object which contained equipartition magnetic fields that generated a highly redshifted Eddington limited secular collapse process. This collapse process was shown to preserve the SPOE by dynamically preventing trapped surfaces, that lead to event horizons, from forming.

In Appendix 1-10 of astro-ph/0505518 it was shown that, by using the Einstein-Maxwell Equations and Quantum Electrodynamics in the context of General Relativistic plasma astrophysics, it was possible to virtually stop and maintain a slow, (many Hubble times!) steady collapse of a compact physical plasma object outside of its Schwarzschild radius.

The non-gravitational force was Compton photon pressure generated by synchrotron radiation from an intrinsic equipartition magnetic dipole field contained within the compact object. The rate of collapse is controlled by radiation at the local Eddington limit, but from a highly redshifted surface.

In Appendix 9 and 10 of astro-ph/0505518, it was shown that general relativistic surface drift currents within a pair plasma at the MECO surface can generate the required magnetic fields. In particular it was shown in Appendix 9 that the equatorial poloidal magnetic field associated with a locally Eddington limited secular rate of collapse of the exterior surface was shown to be strong enough to spontaneously create bound electron-positron pairs in the surface plasma of the MECO. In the context of the MECO highly redshifted Eddington limited balance, the action of this QED process was shown to be sufficient to stabilize the collapse rate of the MECO surface.

For the case of hot collapsing radiating matter associated with the MECO, the corresponding exterior solution to the Einstein equation has been shown to be described by the

time dependent Vaidya metric where no coordinate transformation between MECO Vaidya metric and the Black Hole Kerr-Schild metric exists. Since the highly redshifted MECO Vaidya metric solutions preserve the SPOE they do not have event horizons, and in addition they exhibit a distantly observed slowly rotating intrinsic magnetic dipole moment which interacts with a surrounding accretion disk. Hence the MECO magnetic moments will have observable effects which distinguish them from Black Holes if such MECO exist at the centers of galactic black hole candidates and AGN.

#### ACKNOWLEDGEMENTS

The authors wish to thank Alan Bridle, of the National Radio Astronomy Observatory (NRAO) in Charlottesville Virginia, for many important conversations and analytical discussions which played a key role in clarifying the ideas presented in this paper. In particular one of us (DL) thanks him for graciously allowing access to the research facilities of NRAO during the important developmental phase of this work.

## REFERENCES

- Belloni, T. 2007, Mem. S.A.It, 75, 282
- Chartas, G. et al, 2002, ApJ, 565, 96
- Dai, X. et al, 2004, ApJ, 605, 45
- Elvis, M., 2000, ApJ, 545, 63
- Elvis, M., 2006, Mem.S.A.It 77, 573; astro-ph/0606100
- Elvis, M., 2003, A.S.P.C., 311, 109; astro-ph/0311436
- Falco, E. et al, 1996, AJ 112, 897
- Igumenshev, I. Narayan, R. and Abramowicz, M., 2003, ApJ, 592, 1042
- Illarianov, A. & Sunyaev, R. 1975 A&A 39, 185
- Koptelova, E. et al, 2004, MNRAS, 356, 323
- Landau, L. & Lifshitz, E, 1975, Classical Theory of Fields, 4'th edition, p. 248 - 252
- Leiter, D. and Robertson, S. 2003, Found. Physics Lett. 16, 143
- Lehar, J. et al, 1992, ApJ, 384, 453
- Minezaki, T. et al, 2004, ApJ, 600, L35
- Peterson, B. et al (64 authors), 1991, ApJ 368, 119
- Peterson, B. et al, 1993, ApJ, 392, 470
- Popovic, L. et al, 2006, ApJ, 637, 620
- Robertson, S., and Leiter, D. 2002, ApJ, 565, 447
- Robertson, S., and Leiter, D. 2003, ApJ, 596, L203
- Robertson, S., and Leiter, D. 2004, MNRAS, 350, 1391
- Robertson, S., and Leiter, D. 2005, “The Magnetospheric Eternally Collapsing Object (MECO) Model of Galactic Black Hole Candidate Candidates and Active Galactic Nuclei”, pp1 - 45 (In New Directions in Black Hole Research, ed. P.V.Kreitler, Nova Science Publishers, Inc, ISBN 1-59454-460-3, novapublishers.com

- Romanova, M. et al, 2002, ApJ, 578, 420
- Romanova, M. et al, 2003a, ApJ, 588, 400
- Romanova, M. et al, 2003b, ApJ, 595, 1009
- Romanova, M. et al, 2004, ApJ, 616, L151
- Schild, R. E. 2004, astro-ph/0409549
- Schild, R. E. 2005, AJ, 129, 1225 (S05)
- Schild, R. Leiter, D. & Robertson, S. 2006, AJ, 132, 420 (SLR06)
- Schild, R. E., & Thomson, D. J., 1995, AJ, 109, 1970
- Schild, R. E., & Thomson, D. J., 1997, AJ, 113, 130
- Schild, R. E., & Vakulik, V., 2003, AJ, 126, 689 (SV03)
- Schmidt, R. and Wambsganss, J., 1998, A&A, 335, 379
- Spitovsky, A., 2006, ApJ, 648, L51
- Suganuma, M., et al, 2004, ApJ, 612, L113
- Swain, M. et al, 2003, ApJ, 596, L166
- Uzdensky, D., 2002, ApJ 572, 432
- Uzdensky, D., 2006, astro-ph/0607656
- Vakulik, V. et al, 2006, A&A, 447, 905
- Vakulik, V. et al, 2007, astro-ph/07081082
- Wozniak et al. (2000), Ap.J., 529, 88

Table 1: MECO-QUASAR MAGNETOSPHERIC EQUATIONS - (RL-LHS) AND (RQ-HSS) - [ref. Astr J. v132,420,(2006) and astro-ph/0505518]

MECO Physical Quantity	Equation	Scale
Surface Redshift -	$1 + z_s = 1.5 \times 10^8 (M/7)^{1/2}$	$M^{1/2}$
Surface Luminosity -	$L_s = L_{Edd} / (1 + z_s)$ erg/s	$M^{1/2}$
Surface Temp. -	$T_s = 2.3 \times 10^7 / [M(1 + z_s)]^{1/4}$ K	$M^{-3/8}$
Rotation Rate (1/Tyear) -	$\nu = 2.8 [L_{q,32}/M]^{0.763} / L_{c,44}$ cyl/year	$M^{-1}$
Quiescent Lum. -	$L_{q,32} = 0.65 M [L_{c,36}/M]^{1.75}$ erg/s	$M$
Co-rotation Radius -	$R_c = 46.7 R_g / [M\nu_2]^{2/3}$ cm	$M$
Light Cylinder Radius -	$R_{lc} = [1.52 (Tyear) \times 10^{17}]$ cm	$M$
Magnetic Moment -	$\mu_{27} = 8.16 [L_{c,36} M / \nu_2^3]^{1/2}$ gauss-cm <sup>3</sup>	$M^{5/2}$
Magnetic Field -	$B_\theta = 1.12 (R_g/r)^3 [L_{c,36} / (M^5 \nu_2^3)]^{1/2}$ gauss	$M^{-1/2}$
Magnetosphere Radius (RL-LHS) -	$R_m = 17 R_g [M\nu_2]^{4/21} / (L_{disk}/L_{Edd})^{2/7}$ cm	$M$
Magnetosphere Radius (RQ-HS) -	$R_m = R_{ms}$	$M$
Core X-ray Luminosity -	$L_x = (\eta_{x-corona-disk}) L_{disk}$ erg/s	
Core Radio Luminosity -	$L_{rad,36} = C_{rad-x} M^{0.75} L_{x,36}^{2/3}  1 - (L_{x,36}/L_{c,36})^{1/3} $ erg/s	$M^{3/2}$

In Table 1:

a) the left hand column summarizes the MECO physical quantities relevant to Q0957 and Q2237.

b) the middle column gives the specific form of the equations to be used in the calculation of these specific physical quantities and;

c) the right hand column gives the functional form of the relevant mass scaling of these specific physical quantities in order to demonstrate clearly how the equations for these physical quantities can be applied to the case of both GBHC, AGN and QSO.

Then using the observed values of the X-ray luminosity, radio luminosity, red shift and the physical dimensions of the internal structure seen in Q0957 and Q2237 as input in the MECO equations in Table 1, the results shown in Table 2 are obtained.

Table 2: QUASAR Q2237 (RQ-HSS) VERSUS QUASAR Q0957 (RL-LHS)

MECO Parameters	QUASAR 2237 (RQ-HSS)	QUASAR Q0957 (RL-LHS)
MECO Mass	$3.0 \times 10^9 M_\odot$	$4.2 \times 10^9 M_\odot$
MECO Magnetic Moment	$7.8 \times 10^{51}$ gauss-cm <sup>3</sup>	$1.8 \times 10^{52}$ gauss-cm <sup>3</sup>
MECO Magnetic Field	$(4.0 \times 10^5 \text{ gauss})(3Rg/r)^3$	$(3.4 \times 10^5 \text{ gauss})(3Rg/r)^3$
MECO a/M Ratio	$\sim 0.5$	$> 0.7$
MECO Surface Redshift	$3.1 \times 10^{12}$	$3.7 \times 10^{12}$
MECO Rotation Period - Tyears	5.6 Years	1.6 Years
MECO Surface Luminosity	$1.3 \times 10^{35}$ erg/sec	$1.5 \times 10^{35}$ erg/sec
MECO Surface Temp	74 K	66 K
MECO Co-rotation Radius	$151R_g$	$53R_g$
MECO Light Cylinder-cm	$R = 1867R_g = 8.4 \times 10^{17}$	$R = 383R_g = 2.4 \times 10^{17}$
Accretion Disk Luminosity	$6.2 \times 10^{45}$ erg/sec	$4.6 \times 10^{45}$ erg/sec
Eddington Ratio	0.02	$9.0 \times 10^{-3}$
Core X-ray Luminosity (OBS)	$1.4 \times 10^{44}$ erg/sec	$2.5 \times 10^{45}$ erg/sec
Core Radio Luminosity (OBS)	$1.0 \times 10^{40}$ erg/sec	$3.7 \times 10^{42}$ erg/sec
Core X-ray Efficiency	$\eta_{x\text{-corona-disk}} = 0.03$	$\eta_{x\text{-corona-disk}} = 0.54$
Core Radio X-ray Luminosity Coeff.	$C_{rad-x} = 2.8 \times 10^{-9}$	$C_{rad-x} = 3.5 \times 10^{-7}$
Rm Magnetosphere-cm (OBS)	$R_m = 4.2R_g = 1.9 \times 10^{15}$	$R_m = 64R_g = 4 \times 10^{16}$
Rm Emission Wavelength (OBS)	$2000A_o$	$2697A_o$
Hot Annular Ring at Rm-cm (OBS)	$\delta(R_m) = 0.025R_g = 1 \times 10^{13}cm$	$\delta(R_m) = 1.0R_g = 5.4 \times 10^{14}$
Base of Radio Jet-cm (OBS)	NONE-COMPACT SOURCE	$R = 2 \times 10^{16} H = 9 \times 10^{16}$
Elvis Outflow Structure-cm (OBS)	$R = 8.2 \times 10^{17} H = 1.6 \times 10^{17}$	$R = 2 \times 10^{17} H = 5 \times 10^{16}$

In Table 2 the data presented is intended to be read as follows:

The scaling relations from Table 1 and other input data are used to determine the properties of Q2237 in the Radio Quiet High Soft State and Q0957 in the Radio Loud Low Hard State. We emphasize in the lower rows the model derived predicted values of observable parameters, principally the observable size scales. However many of these size scales have already entered the MECO model calculations, but are repeated here for a complete listing of observable and physical properties.



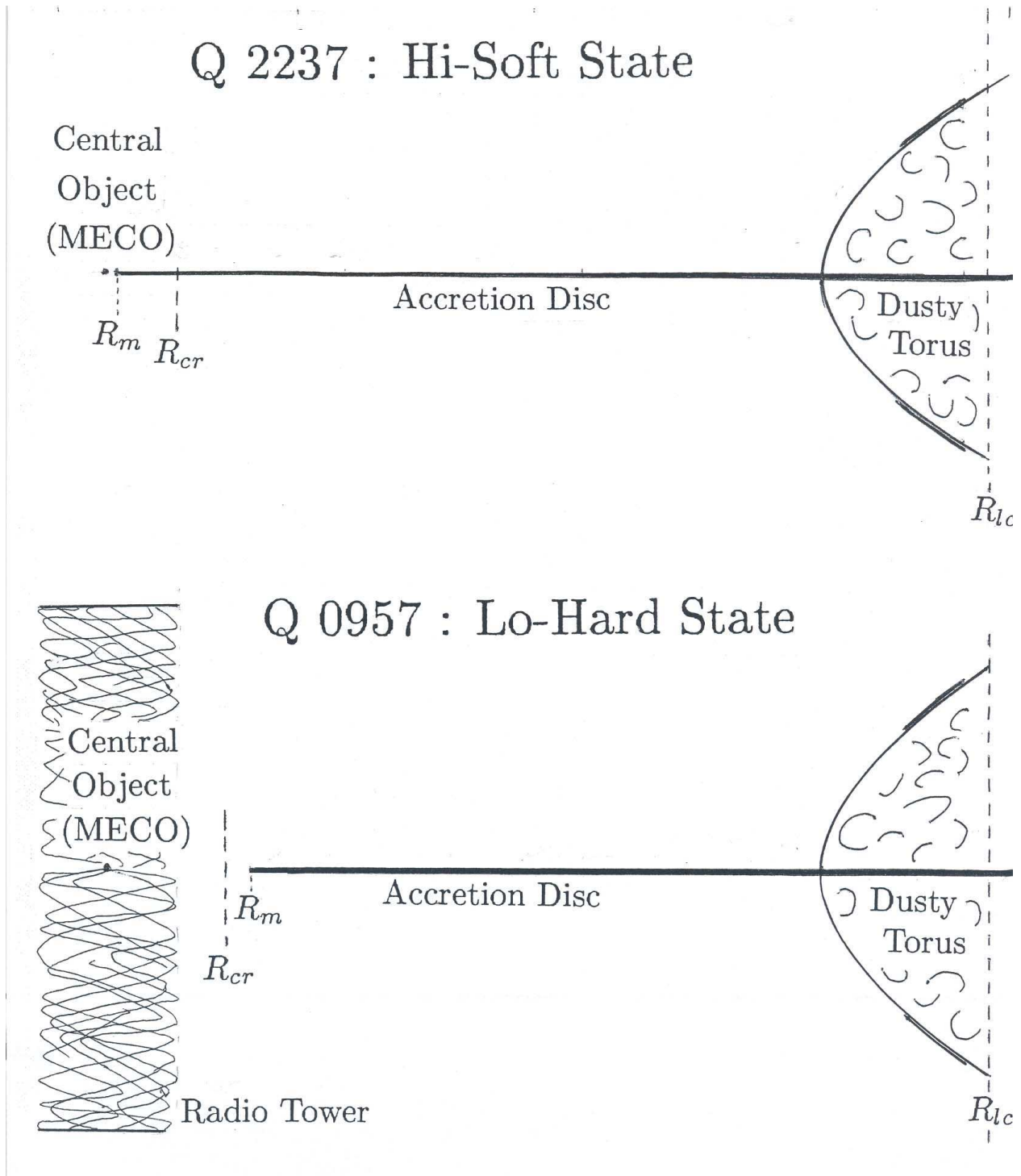


Fig. 1.— A cross-section view comparing the structures of two quasars with structure determined by microlensing-reverberation analysis. For both quasars, the compact central object (MECO) is a small dot on the left, and to its right is the accretion disc plane for the right-hand side of the quasar. To aid comparison of the visible structures, both have been scaled to make the distance from the central object to the light cylinder and Elvis structure the same, although in reality the Q2237 quasar is  $\times 3.5$  larger. Labels show the locations of the magnetic radius ( $R_m$ ), the co-rotation radius ( $R_{cr}$ ), and the light cylinder radius ( $R_{lc}$ ). The UV-optical luminous structures are the bright band at the inner edge of the accretion disc

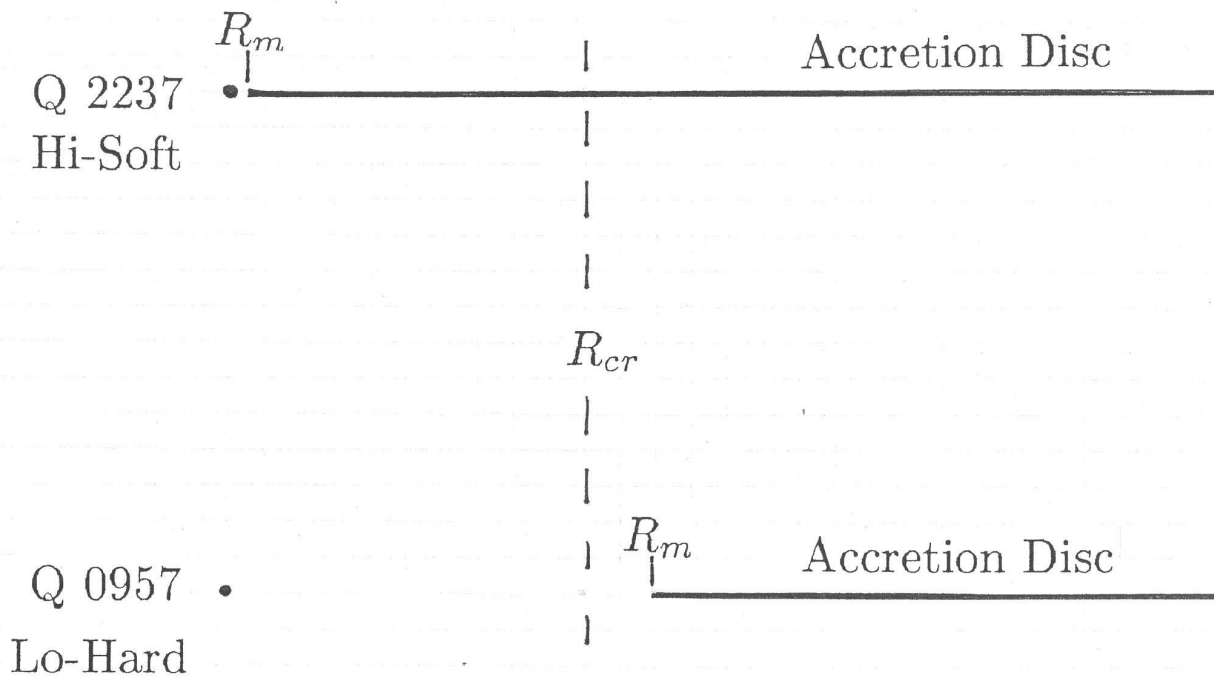


Fig. 2.— A cartoon showing comparison of the inner structure of the two quasars, emphasizing the important relationship of the magnetospheric radius  $R_m$  (at the inner edge of the accretion disc), to the co-rotation radius  $R_{cr}$ , which is where the Keplerian orbital speed equals the sweeping magnetic field speed. For this comparison the two quasars have been rescaled to have the same co-rotation radius  $R_{cr}$  to emphasize how the accretion disc in Q2237 penetrates almost to the central MECO because of its higher accretion rate, whereas in Q0957 its luminous inner edge is outside of co-rotation. This difference is the physical reason for the difference in spectral states between the two quasars.